Paper A

Influence of Variable Froude Number on Waves Generated by Ships in Shallow Water.

Influence of variable Froude number on waves generated by ships in shallow water

Tomas Torsvik and Kristian Dysthe
Department of Mathematics, University of Bergen,
Johannes Brunsgate 12, NO-5008 Bergen, Norway

Geir Pedersen
Department of Mathematics, University of Oslo,
PO Box 1053, Blindern, NO-0316 Oslo, Norway

Abstract

Passage through the transcritical speed region of a moving disturbance in a shallow channel, is examined using numerical simulations based on a set of forced Boussinesq equations. The transition is accomplished either by accelerating the wave generating disturbance in a region of constant depth or by moving the disturbance with constant speed over a sloping bottom topography. A series of test cases are examined where the transcritical region is traversed both from subcritical to supercritical speed and vice versa. Results show that the generation of upstream solitary waves depends on the time required for the transition, with large waves being generated for long transition times. It is also apparent that the shape of the wave pattern, and the maximum amplitude of the waves, differ significantly depending on whether the Froude number increase or decrease during the transition of the transcritical region. However, the wave pattern is not determined simply in terms of the Froude number. The strength of the forcing term as well as the underlying process which cause the Froude number to vary, i.e. acceleration and depth variation, influence the wave pattern in different ways. The Froude number is none the less a useful indicator for the problem, since all cases with similar Froude number variation share some common characteristic features.

I. INTRODUCTION

It is well known that large, high-speed vessels moving at near-critical speeds in shallow water, can generate long, finite amplitude waves. These waves differ from the wake waves generated by conventional ships, and may constitute an environmental and safety hazard in confined waters. Field studies have been carried out on several locations where problems of this nature have occurred (for an overview, see Parnell and Kofoed-Hansen[1] and the references therein). A characteristic feature in the wave pattern is the occurrence of one or more solitary waves which are generated upstream of the vessel, and are often seen leading the wave packet as the waves approach the shore (see Miles[2] for a general review on solitary waves). The evolution of the waves in the far-field is often examined numerically using long wave models based on the forced Boussinesq (fB) equations or the forced Korteweg-deVries (fKdV) equation, where a localized pressure disturbance is included to represent the ship (see Li and Sclavounos[3] and the references therein). Most of these studies include only cases where the depth h, and the speed of the ship U, are maintained at constant values, and hence the depth Froude number $F = U/\sqrt{gh}$, is also constant. There are however a few articles which considers effects due to a variable Froude number.

Kevorkian and Yu[4] studied the transition through the critical speed region using a method based on asymptotic expansions and subsequent matching of the solutions in the sub-, trans- and supercritical flow regions .The expansion for the transcritical region was valid for a time interval which depended on the magnitude of the forcing term, which limited the study to fairly short transition times. The authors presented analytical and numerical results for flows in the non-dispersive limit. Redekopp and You[5] studied a problem involving a variable Froude number using the fKdV equation. The disturbance travelled at supercritical speed at the start and end of the simulations, but entered the transcritical region during some intermediate time interval. Grimshaw et al.[6] constructed an asymptotic model based on the fKdV equation, and applied this to examine the interaction of solitary waves with an external forcing moving with constant acceleration. The article included an elaborate account of the trapping of solitary waves by the forcing, where the solitary wave was localized close to the forcing and is influenced by the forcing over a long time interval. While the wave propagation in the above mentioned articles was restricted to one horizontal dimension, Jiang et al.[7] investigated waves on a 2D free surface, generated by a ship moving on a fairway of varying topography. The numerical model used in the article combined a slender-body representation of the ship with Boussinesq equations for waves propagating in the far-field.

Although the effect of a variable Froude number is examined in these articles, none of the articles give a comprehensive description of the wave pattern generated during the transition through the transcritical speed region for a wide range of parameters. In the present paper we examine the transition problem, restricted to waves propagating in one horizontal dimension, but allow for a wide range of parameters. This way we hope to provide a more complete account of the processes which influence the wave pattern when a ship accelerates or decelerates while it is close to the critical speed region.

The equations are presented in §II, along with the numerical method which has been applied for the simulations. Results for numerical simulations with a variable Froude number are presented in §III, and concluding remarks are given in §IV.

II. EQUATIONS AND NUMERICAL METHOD

The equations are formulated in a coordinate system with one horizontal axis x^* and the vertical axis z^* with zero at the equilibrium free surface. The asterisk indicates dimensional quantities. The fluid is confined to the region $-h^* < z^* < \eta^*$, where $h^*(x^*)$ is the depth of fluid at equilibrium, and $\eta^*(x^*, t^*)$ is the position of the free surface. We assume that the fluid is irrotational and incompressible, and that vertical processes evolve on a slow time scale, which allows us to formulate the equations in terms of the depth integrated velocity potential $\phi^*(x^*, t^*)$. Waves are generated by allowing an external pressure $p^*(x^*, t^*)$ of constant form and magnitude, to act on the free surface. All functions and variables in the equations are made dimensionless by the transformation

$$\begin{aligned} z^* = h_0 z \qquad x^* = lx \qquad t^* = l(gh_0)^{-\frac{1}{2}} t \qquad h^* = h_0 h(x) \\ \eta^* = \alpha h_0 \eta(x,t) \qquad \phi^* = \alpha l (gh_0)^{\frac{1}{2}} \phi(x,t) \qquad p^* = \alpha \rho g h_0 p(x,t) \end{aligned} \tag{1}$$

where h_0 is a typical depth, l is a typical wavelength, g is the acceleration of gravity, ρ is the fluid density and α is a small parameter.

The derivation of the Boussinesq equations from the primitive equations is well documented, see e.g. Wu[8], and we have used the forced Boussinesq equations of the form

$$\begin{aligned} &\eta_t + \left[(h + \alpha\eta)\phi_x + \epsilon h h_x \left(\frac{1}{6}\eta_t - \frac{1}{3} h_x \phi_x \right) \right]_x = 0 \,, \\ &\phi_t + \eta + p + \frac{1}{2}\alpha \left(\phi_x\right)^2 - \epsilon \left(\frac{1}{2} h \left[h \phi_{xt} \right]_x - \frac{1}{6} h^2 \phi_{xxt} \right) = 0 \,, \end{aligned} \tag{2}$$

which allows for a sloping bottom topography, as demonstrated by Pedersen[9]. The parameters

$$\alpha = \frac{a^*}{h_0} \,, \qquad \epsilon = \frac{h_0^2}{l^2} \,,$$

where a^* is a typical wave amplitude, are measures of nonlinearity and dispersion, respectively, and they are both required to be small in order for the equations to be accurate.

The ship is represented by a localized perturbation of the pressure at the free surface. Since the model is not suited to study the detailed flow near the hull of the ship, we have not attempted to include a realistic representation of a ship in the model, and have instead used a simple function to determine the pressure disturbance, which is given by

$$p(x,t) = \begin{cases} P_0(t) \cos^2 \left(\frac{\pi}{L} \left(x - x_p(t) \right) \right) & -\frac{L}{2} \le \left(x - x_p(t) \right) \le \frac{L}{2} \\ 0 & \text{elsewere} \end{cases} \,, \tag{3}$$

where $P_0(t)$ is the amplitude, L is the length and $x_p(t)$ is at the centre of the pressure disturbance.

The moving disturbance will experience a resistance to the motion due to wave generation and radiation. A measure of this resistance is expressed by the wave drag

$$D_W = -\int_{-\infty}^{\infty} p(x,t)\, \eta_x dx \,.$$

Both upstream and downstream waves contribute to the wave drag, but the major time variation is contributed by the generation of upstream waves, as shown by Lee et a.[10].

A. Numerical method

The scaling introduced above is convenient when discussing the equations, but can obscure the readability of the numerical results. We therefore introduce new dimensionless variables where all lengths are scaled with the reference depth h_0 and the time unit is the time required to travel the distance of the depth with the linear shallow water speed. This amounts to replacing l with h_0 and removing the scaling parameter α when defining the dimensionless variables (1). The fB equations formulated in terms of the new dimensionless variables have the same form as equations 2, except the parameters α and ϵ no longer appears explicitly in the formulation. Naturally, the content and performance of the equations are not altered by this re-scaling.

The equations are solved numerically using a finite difference method. The solution of the Boussinesq equations follows Pedersen[9], and only the main features are presented here. A quantity f is approximated at grid points with coordinates $(\beta\Delta x, \kappa\Delta t)$, where Δx and Δt are grid increments, and is denoted $f_\beta^{(\kappa)}$ in the difference equations. The equations are solved on a grid which is staggered in both space and time, where η is evaluated at grid points and ϕ is evaluated at staggered points, i.e.

$$\eta(\beta\Delta x, \kappa\Delta t) \approx \eta_\beta^{(\kappa)}, \qquad \phi\left((\beta+\tfrac{1}{2})\Delta x, (\kappa+\tfrac{1}{2})\Delta t\right) \approx \phi_{\beta+\frac{1}{2}}^{(\kappa+\frac{1}{2})}.$$

Derivatives are approximated by central differences in both space and time, resulting in implicit formulations for the time evolution of both η and ϕ. Each time step involves solving two tri-diagonal propagation matrices.

The solution is calculated on a large spatial domain in order to avoid interference of noise from lateral boundaries with the main part of the wave pattern. This does not involve an extensive computational cost, since the equations only have one spatial dimension. Our only concern has been to avoid blow up of noise at the boundaries, and we have therefore implemented simple boundary conditions which reflect incoming waves.

It is not a straight forward task to analyze a nonlinear model for stability. Our choice of time stepping in the simulations, $\Delta t = 0.8\,\Delta x$, is based on the analysis of the linearized model equations, which is outlined in Pedersen[9]. We have not experienced numerical instabilities in any of the simulations with this model, provided the value of Δx was within a reasonable range. The numerical scheme has been tested for convergence by grid refinement. The same simulation was executed on spatial grids with increments Δx of 0.5, 0.25 and 0.125, and the error, in L_2 norm, of η at the end of each simulation was calculated, using the fine grid result as the true solution. The current numerical scheme is formally of 2nd order, and the grid refinement test gave an order of convergence of 1.8961. Based on this result, we conclude that the numerical solution converges when we use a spatial resolution of $\Delta x = 0.125$, and this value has been used in all the simulations hereafter.

III. RESULTS FOR VARIABLE FROUDE NUMBER

Variations in the speed U of the ship and the water depth h influence the value of the Froude number, but changes in these two variables does not induce the same variation, neither in the Froude number nor in the problem as a whole. We wish to examine the effect of variation in both these variables in separate test cases; one where the ship accelerates at the constant acceleration G in a region of constant depth, and one where the ship moves at constant speed in a region where the bottom has a slope of constant inclination S.

Simulations for the two test cases have been set up to be as similar as possible. A spin up period for the pressure amplitude of 50 time units is used, while U and h are kept constant. The initial values of U and h correspond to either sub- or supercritical cases, but close to being in the transcritical region. Variation of the Froude number is initiated at $t = t_1 = 100$. In the case of a sloping bottom topography, this is achieved by carefully choosing the initial position of the pressure disturbance relative to the position of the slope. The ship proceeds through the transcritical flow region, and the Froude number continues to change until it reaches a specific value at some time $t = t_2$. Thereafter both the speed U and the depth h are maintained at constant values.

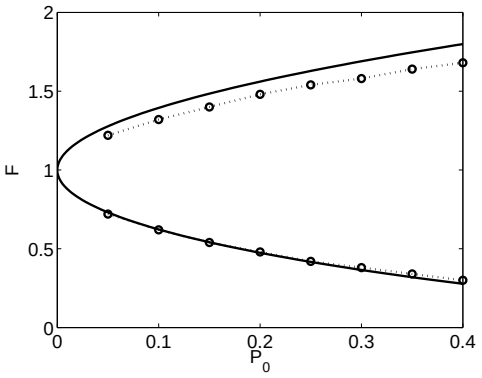

FIG. 1: Limits for bore and soliton generation. Results are shown for the NLSW model (solid line) and the Boussinesq model (dotted line with circles).

The approach described above requires some knowledge about the extent of the transcritical region. This problem has been studied by Houghton and Kasahara[11] for flow over a disturbance at the bottom, within the context of the nonlinear shallow water (NLSW) equations (without dispersion). Although the NLSW model give qualitatively incorrect results for the flow over a bump, as demonstrated by Nadiga et al.[12], it nevertheless provides a reasonable estimate for deciding the boundaries for the transcritical flow. Figure 1 show the limits for bore generation predicted by the NLSW model together with limits found for the generation of an undular bore or a solitary waves using the fB model with a pressure disturbance. The results for the Boussinesq equation is based on visual inspection of results from simulations with constant Froude numbers, and has a margin of error of approximately $F = \pm 0.02$. The limits found for the fB equations determine what is considered to be the transcritical region in the rest of this article.

A. Constant acceleration

In the first test case the speed of the ship accelerates with a constant acceleration $G = dU/dt$, while the depth remains constant. In terms of dimensional variables the acceleration is determined by $G = g^{-1}\, dU^*/dt^*$, i.e. as the ratio of the ship's acceleration to the acceleration of gravity. By choosing the constant depth $h = 1$, and imposing constant acceleration, the time dependence of the Froude number during acceleration is determined by

$$F(t) = G(t - t_1) + U(t_1)\,, \qquad t_1 < t < t_2\,.$$

Figure 2 shows the time development of the wave pattern and wave drag for a pressure disturbance of amplitude $P_0 = 0.05$ and length $L = 10.0$, which accelerates from $F = 0.7$ to $F = 1.7$. The pressure disturbance is moving towards the left, and the coordinate system follows the pressure disturbance, which is located at $-5 \leq x \leq 5$. The fluid is moving to the right in the reference frame of the ship. In the last two cases the simulation is stopped once the amplitude of the largest upstream wave has grown to $a = 1$, since this is well above the stability limit of solitary waves ($a = 0.78$), within full potential theory as given by Tanaka[13]. This stopping criteria is also generous in the sense that waves are allowed to develop which are not well represented by weakly nonlinear wave theory. According to Miles[2], weakly nonlinear Boussinesq theory have been shown to fit wave profiles from experiments for waves with amplitudes up to $a \leq 0.5$, but should not be expected to provide correct results for waves with significantly higher amplitudes. In our simulations we demonstrate how large amplitude waves may be generated when the Froude number is allowed to vary, but we do not study how these waves evolve once they are generated. All contour plots have contour lines within the range $[-0.475, 0.475]$, plotted at increments of 0.05. In some cases the waves have amplitudes larger than 0.475, but we do not include contour lines beyond this value because they would be inseparable in the plots.

The magnitude of the acceleration has significant influence on the amplitude of the upstream wave which is generated in the transcritical region. It should be noted that once a wave is generated in the transcritical region, it remains trapped close to the pressure disturbance for Froude numbers which are normally considered to be outside the transcritical region ($F > 1.25$ for $P_0 = 0.05$). When the acceleration is fast, as in Fig. 2(a), a small amplitude wave develops upstream of the pressure disturbance in the transcritical region, and is left behind by the pressure disturbance in the supercritical region. This process is also represented in the wave drag, Fig. 2(b), which is positive in the transcritical region, and turns negative once the pressure disturbance pass the crest of the solitary wave. The negative value in the wave drag corresponds to a situation where the pressure disturbance is located on the upstream slope of the solitary wave, and hence acts as an obstacle for the wave propagation. For smaller values of G, as in Fig. 2(c), the large upstream wave remains confined close to the pressure disturbance until the amplitude grows to $O(1)$. When $G = 0.002$, Fig. 2(e), the upstream bore which is generated at small transcritical Froude numbers is allowed to develop, and eventually breaks up into three separate solitary waves when $F \approx 1.1$. The wave drag increases rapidly when the pressure disturbance enters the transcritical region, and then increase slowly during the initial phase of the upstream wave generation. Once a wave has been developed, and is trapped upstream of the pressure disturbance, the wave drag almost doubles in magnitude, as seen in Fig. 2(d).

Figure 3 shows the wave pattern generated by a deceleration from $F = 1.25$ to $F = 0.7$, for acceleration G of -0.05, -0.01 and -0.002. An upstream wave of moderate amplitude

Fig. 2, Torsvik, Physics of Fluids

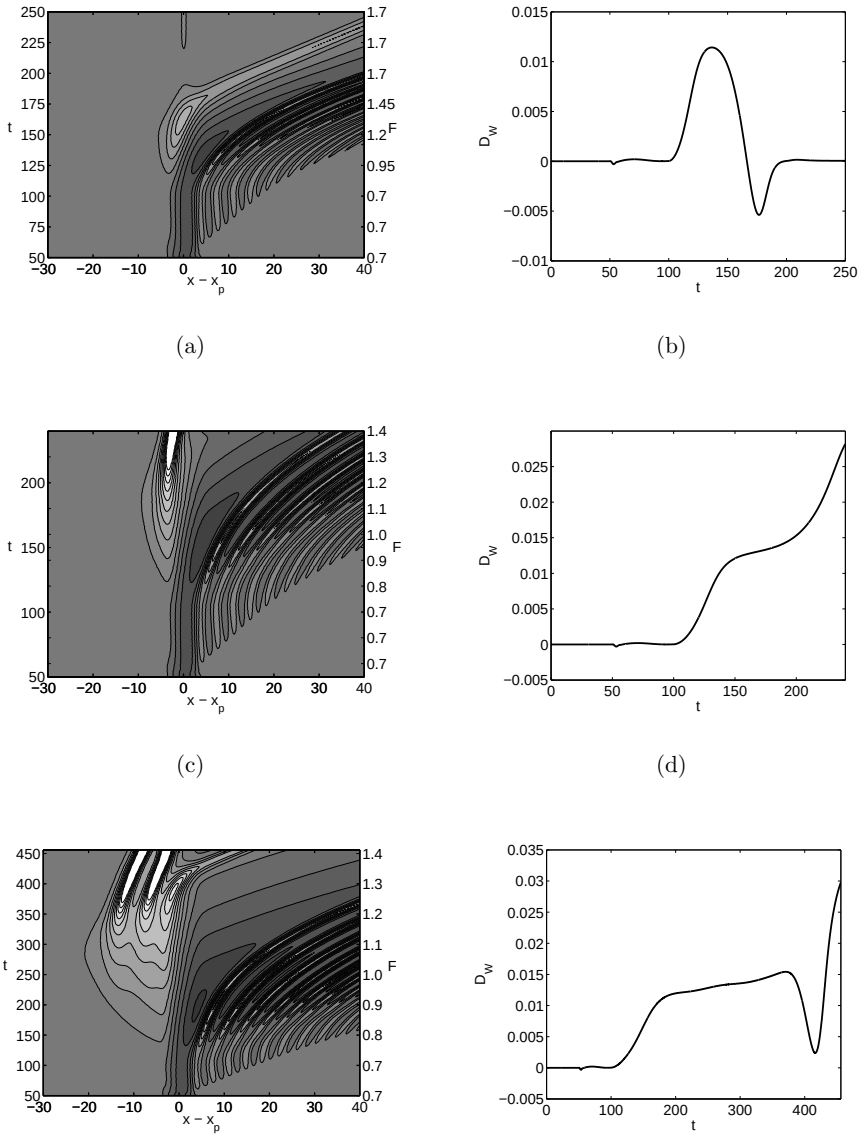

FIG. 2: Time development of wave pattern and wave drag for constant positive acceleration. Results are shown for $G = 0.01$, Figures (a) and (b), $G = 0.005$, Figures (c) and (d), and $G = 0.002$, Figures (e) and (f). Contour lines range from -0.457 to 0.457 by increments of 0.05.

Fig. 3, Torsvik, Physics of Fluids

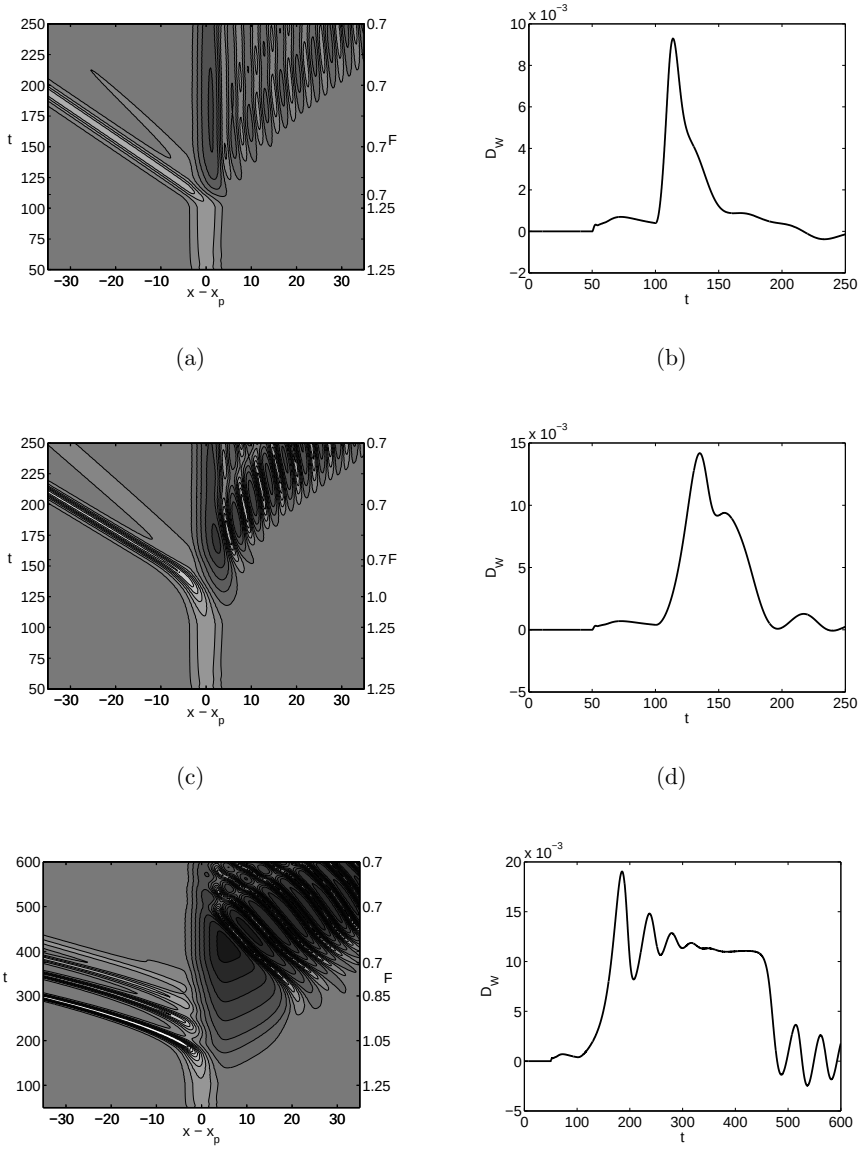

FIG. 3: Time development of wave pattern and wave drag for constant negative acceleration. Results are shown for $G = -0.05$, Figures (a) and (b), $G = -0.01$, Figures (c) and (d), and $G = -0.002$, Figures (e) and (f). Contour lines range from -0.457 to 0.457 by increments of 0.05.

is always generated in the transition from super- to subcritical speed. This is due to the localized and steady elevation on the free surface, which is associated with the pressure disturbance in the supercritical region (see e.g. Cao et al.[14]). In the transcritical region, this elevation will evolve into a solitary wave which eventually propagates upstream of the pressure disturbance. As $G \to 0$, both the amplitude and number of upstream solitary waves increase. The generation of solitary waves is associated with distinct peaks in the wave drag.

Fig. 4, Torsvik, Physics of Fluids

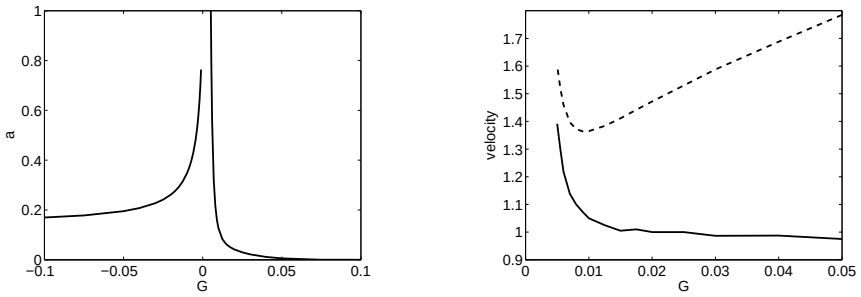

(a) (b)

FIG. 4: Amplitude (a) and speed (b) of the largest solitary wave generated at different accelerations. The stapled line in Figure (b) indicate the speed of the pressure disturbance at the time of zero wave drag.

The amplitude of the largest solitary wave as function of acceleration is shown in Fig. 4(a). We see that a fast acceleration results in a solitary wave with small amplitude, and that the amplitude increases as the the value of G approaches zero. Most of the behaviour evident from this figure can be explained if we consider results from studies of constant Froude number test cases (see e.g. Lee et al.[10]). Since the upstream solitary wave attains its maximum amplitude, for a given Froude number, only after it has travelled with the pressure disturbance for a distance of several depths, a fast acceleration will cause the pressure disturbance to leave the transcritical region before the solitary wave is fully developed. These previous studies also demonstrate that the amplitude of the solitary waves increase with increasing Froude numbers, which explains the increase in amplitude for $G \to 0^-$, since in this case the first solitary wave will be generated while the Froude number is still in the upper part of the transcritical region. The asymmetry in amplitude for the fast acceleration and fast deceleration cases can be attributed to the difference in starting conditions, where in the latter case a steady elevation on the free surface is present near the pressure disturbance.

The increase in amplitude for small, positive values of acceleration is attributed to capturing of the solitary wave by the pressure disturbance. This phenomenon has been described by Grimshaw et al.[6]. If the pressure disturbance is moving with constant speed, then a fully developed solitary wave will propagate upstream of the pressure disturbance. When the pressure disturbance accelerates, it will catch up with the solitary wave. The amplitude and speed of the wave continues to grow, causing the wave to remain in front of the pressure disturbance. Figure 4(b) provides us with an indication for when the trapping of the solitary

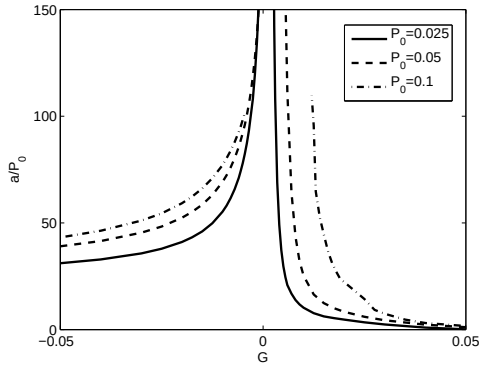

FIG. 5: The ratio of the amplitude of the largest solitary wave to the amplitude of the pressure disturbance for different values of P_0.

wave occurs. In this figure we compare the speed of the largest solitary wave when it has escaped the influence of the pressure disturbance (solid line) with the speed of the pressure disturbance at the time when it stops contributing to the growth of the wave (dashed line). This latter time is determined by the first time of zero wave drag for $t > t_1$, which occurs in all cases where the wave is passed by the pressure disturbance (see Fig. 2(b)). The speed of the pressure disturbance at zero wave drag has a minimum at $G \approx 0.01$, and increase as $G \to 0^+$, indicating that when the acceleration is sufficiently small, the wave is able to follow the pressure disturbance for higher Froude numbers.

Grimshaw et al.[6] found a condition which determines when the trapping of the wave may occur. In terms of variables used in this article, the condition is given by

$$\frac{GL}{\alpha P_0} \leq 2\pi \, .$$

For the test cases shown in Fig. 2, with $P_0 = 0.05$, $L = 10.0$ and $\alpha = 1$, the condition found by Grimshaw et al. predicts trapping for $G \leq 0.0314$, and the simulations show that waves are trapped for $G \approx 0.01$. These results are not necessarily in contradiction, since trapping will only occur at the limit $G = 0.0314$ under highly idealized conditions. Furthermore, the model derived by Grimshaw et al. requires that the wave maintains a perfect soliton shape, and that the wave is long compared to the wave generating disturbance. These conditions are not satisfied in our model.

The constant acceleration case has been studied for pressure disturbances with amplitudes $P_0 = 0.025$, 0.05 and 0.1. Figure 5 shows the amplitude of the largest solitary wave scaled with the amplitude of the pressure disturbance for these three cases. As before, the simulations were stopped once the amplitude of the solitary wave grew to $O(1)$. All three test cases show similar trends, with large amplitude waves being generated at accelerations close to zero. The time required to generate a solitary wave decreases with increasing values of P_0, and hence the trapping mechanism for positive accelerations occurs at larger accelerations for large values of P_0.

The number of solitary waves generated during the transition increases as the acceleration approaches zero, as seen in Fig. 6. The number of waves is generally higher for negative

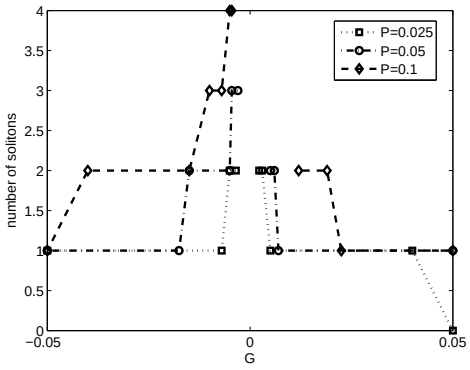

FIG. 6: The number of solitary waves generated at different accelerations.

accelerations than for positive accelerations, and is also influenced by the strength of the pressure disturbance. Redekopp and You[5] attempted to predict the number of waves being generated when passing through the transcritical region. They defined a parameter based on time integration of the Froude numbers for the transition time, but found that this measure was not uniquely correlated to the number of solitary waves. Our results demonstrate that any such measure must take into account the differences in the wave generating process for positive and negative accelerations.

B. Linear depth variation

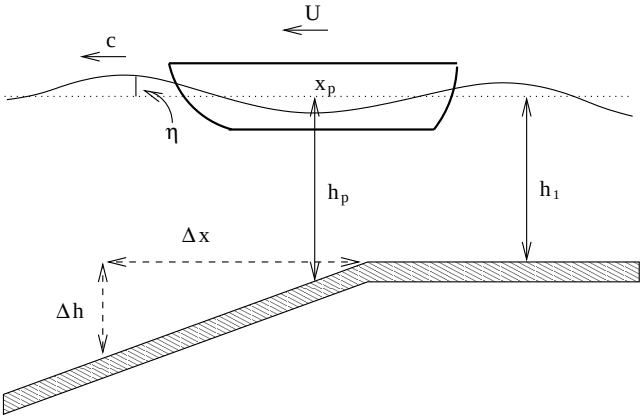

FIG. 7: Sketch of the variable depth problem, including the relevant variables.

For the simulations where a pressure disturbance moves over a sloping bottom topography, we keep the speed of the pressure disturbance constant at $U = 1$, and hence the depth $h = 1$ corresponds to the critical Froude number $F = 1$. The depth at the initial position of the

pressure disturbance, h_1, is constant, and the pressure disturbance reaches the start of the slope at $t = t_1 = 100$. At some later time t_2 the pressure disturbance once again enters a region of constant depth h_2. The slope of the bottom topography is denoted by $S = \Delta h/\Delta x$, see Fig. 7, with the convention that a positive value of S corresponds to decreasing depth. The pressure disturbance experiences that the local depth $h_p(t)$ varies with time, and the time dependence is determined by

$$\frac{dh_p}{dt} = S\,,$$

since $U = 1$. As a result, the Froude number is determined by

$$F(t) = [h_1 - S(t - t_1)]^{-\frac{1}{2}}\,, \qquad t_1 < t < t_2\,,$$

on the slope. The pressure disturbance has amplitude $P_0 = 0.05$ and length $L = 10.0$.

Figure 8 shows results for simulations where the depth decreases from $h_1 = 2.04$ ($F = 0.7$) to $h_2 = 0.346$ ($F = 1.7$). Several features in the wave pattern and wave drag are similar to results for constant acceleration shown in Fig. 2. When the slope is steep, Fig. 8(a), the pressure disturbance is able to pass the upstream bore generated in the transcritical region, which subsequently propagates as a solitary wave downstream. In our simulations we found that the solitary wave was detached from the pressure disturbance after the pressure disturbance had entered the region of constant depth h_2. The amplitude of the solitary wave increases as the inclination of the slope decreases, until it is trapped by the pressure disturbance at about $S = 3.0 \cdot 10^{-2}$. Trapping of the solitary wave does not cause any significant increase in the wave drag, as seen in Fig. 8(d). The amplitude of the solitary wave at the end of the simulation is $a = 0.454$, which is of the same magnitude as the local depth, but still only moderate in view of the amplitude of the pressure disturbance. Multiple solitary waves may be generated if the inclination of the slope is sufficiently small, as seen in Fig. 8(e).

Figure 9 shows results for simulations where the depth increases from $h_1 = 0.574$ ($F = 1.32$) to $h_2 = 1.778$ ($F = 0.75$). The range of the transcritical region is slightly shifted compared to the deceleration case because the impact of a pressure disturbance changes due to the variation in depth, even though the amplitude P_0 remains constant. Once again we see that the wave pattern and wave drag have similar features when compared to results for constant deceleration, Fig. 3. During the transition through the transcritical region, a depression of the free surface is formed downstream of the pressure disturbance. When the pressure disturbance reaches the region of constant depth h_2, a slight depression is formed upstream, which persists until the trailing waves catch up with the pressure disturbance. At this point, the interaction between the pressure disturbance and the trailing waves may result in further generation of upstream waves, as seen in Fig. 9(e).

We wish to compare the upstream waves generated by the disturbance for different slope inclinations. Since the waves are constantly changing while moving over the sloping bottom topography, we need a criterion to determine the time for which the wave is no longer influenced by the forcing disturbance. This is achieved by comparing the result from the simulation, for each time step, with a simplified case where the upstream wave is replaced by an exact soliton solution with equal amplitude a, and determine the time of detachment from the distance between the soliton and the forcing disturbance, see Fig. 10. We consider the solitary wave to be independent of the forcing disturbance when the exact soliton solution is reduced to $0.01a$ at the location of the forcing disturbance. This method has been applied

Fig. 8, Torsvik, Physics of Fluids

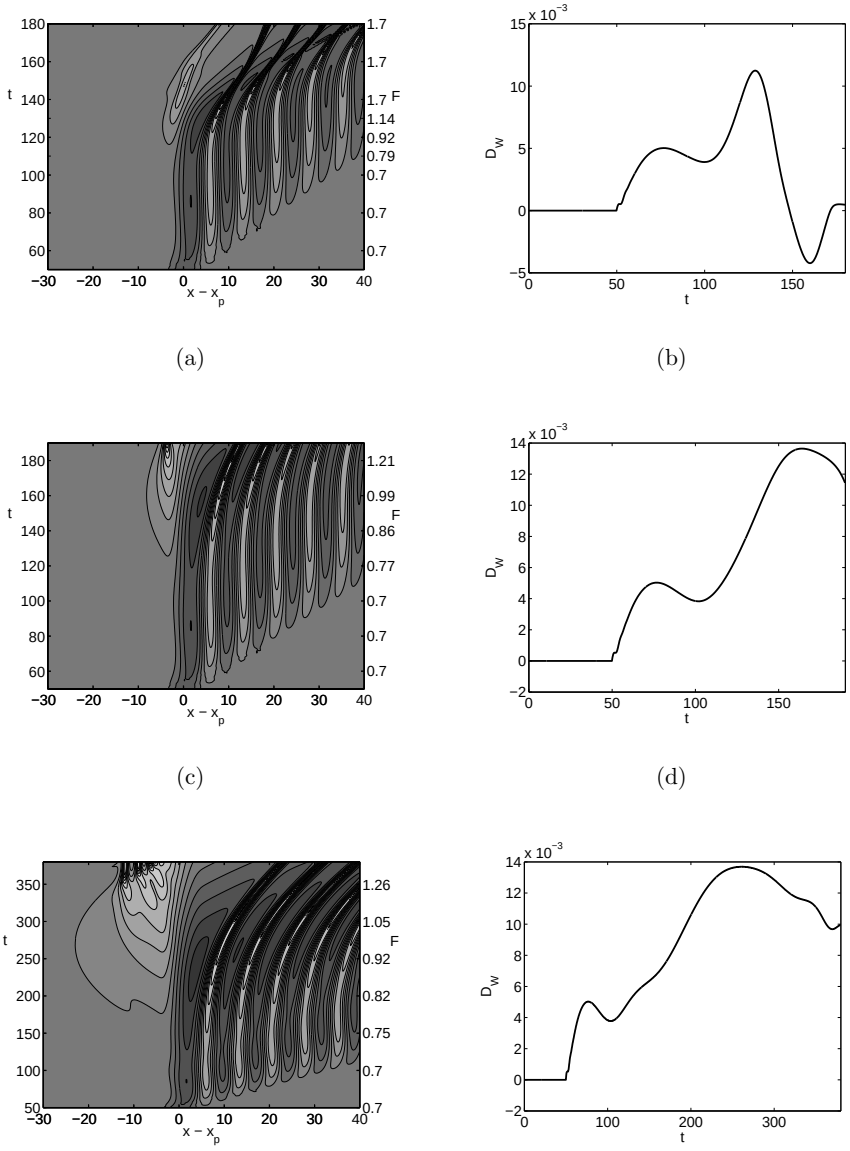

FIG. 8: Time development of wave pattern and wave drag for linear decreasing depth. Results are shown for $S = 4.23 \cdot 10^{-2}$, Figures (a) and (b), $S = 1.69 \cdot 10^{-2}$, Figures (c) and (d), and $S = 5.65 \cdot 10^{-3}$, Figures (e) and (f). Contour lines range from -0.457 to 0.457 by increments of 0.05.

Fig. 9, Torsvik, Physics of Fluids

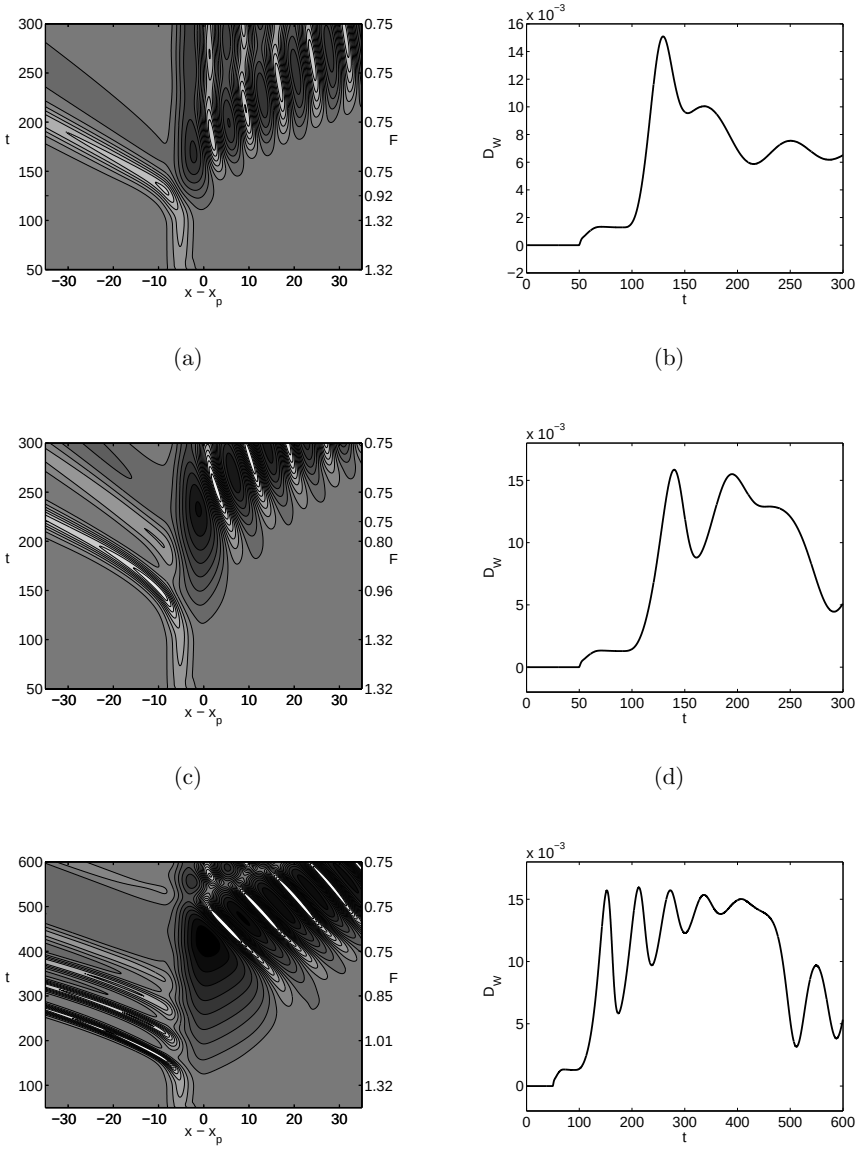

FIG. 9: Time development of wave pattern and wave drag for linear increasing depth. Results are shown for $S = -2.41 \cdot 10^{-2}$, Figures (a) and (b), $S = -1.00 \cdot 10^{-2}$, Figures (c) and (d), and $S = -4.01 \cdot 10^{-3}$, Figures (e) and (f). Contour lines range from -0.457 to 0.457 by increments of 0.05.

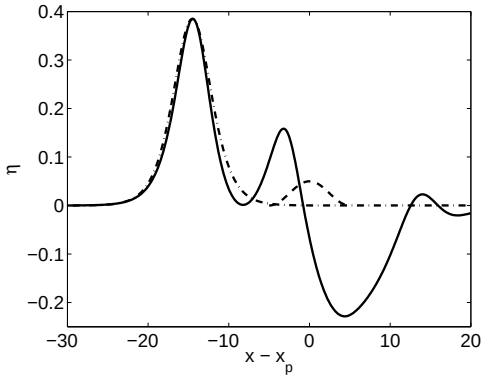

FIG. 10: Leading wave detachment determined by comparison with soliton solution. The figure shows the free surface (solid line), the soliton (dash-dot line), and the pressure disturbance (dashed line).

to the cases of increasing depth, and a graph of the amplitude of the waves for different sloping inclinations is shown in in Fig. 11. We see that the amplitude increases as the slope inclination becomes smaller, which is in agreement with similar results for a decelerating pressure disturbance. When the inclination of the slope is small, the leading solitary wave is detached from the pressure disturbance while it is still on the slope, but for steep slopes the upstream wave is only generated after the pressure disturbance has reached the region of constant depth h_2. The transition between these two regimes occurs at approximately $S = -0.01$, and is reflected in the kink seen in Fig. 11 for this value.

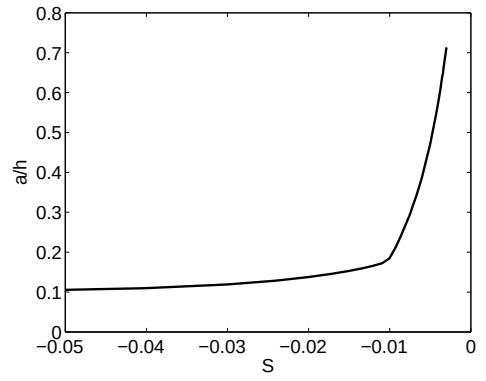

FIG. 11: Amplitude of solitary waves for a forcing disturbance moving over a sloping bottom of increasing depth.

IV. CONCLUDING REMARKS

In this article we have studied waves generated by a moving pressure disturbance in shallow waters, with focus on variable Froude number effects. The study shows features which are not present when the Froude number is constant. We also find that it is important to distinguish between the cases of increasing and decreasing Froude number.

Moving from super- to subcritical speed always generates a solitary wave with significant amplitude. When the transition is fast, the generation of the solitary wave is largely due to the supercritical solution attained at the start of the simulation, where a steady elevation on the surface is located at the position of the forcing disturbance. A slow transition allows the solitary wave to fully develop and propagate upstream while the forcing disturbance is still in the transcritical region. The leading solitary wave becomes larger as the transition time increases, because the large transition time allows the solitary wave to fully develop while in the upper part of the transcritical region, where a larger wave celerity, and hence larger wave amplitude, is needed in order for the wave to escape the influence of the forcing disturbance.

The amplitude of the solitary wave generated during a transition from sub- to supercritical speed is highly dependent on the transition time. Since the free surface is not elevated near the forcing disturbance in the initial state of subcritical speed, the generation of solitary waves depends entirely on the transition process. While in the transcritical region, the forcing disturbance creates a net mass flux from the downstream to the upstream region. A fast transition prevents this process from being sustained over a long time interval, in which case no solitary wave of appreciable amplitude evolves close to the pressure disturbance. Increasing transition times results in the generation of an upstream bore. For intermediate transition times the forcing disturbance is able to overtake the bore, which is subsequently reduced in amplitude and transformed into a solitary wave downstream. When the transition time is long, the amplitude of the upstream bore grows until it is of the same magnitude as the depth, which is beyond the maximum amplitude acceptable for the model.

Acknowledgements

This work has received support from The Research Council of Norway through a grant to the program “Modelling of currents and waves for sea structures”. The authors thank two anonymous reviewers for constructive comments, which lead to a substantial improvement of the paper.

[1] K. E. Parnell and H. Kofoed-Hansen, "Wakes from large high-speed ferries in confined coastal waters: Management approaches with examples from New Zealand and Denmark", Coast. Manage. **29**, 217–237 (2001).

[2] J. W. Miles, "Solitary waves", Ann. Rev. Fluid Mech. **12**, 11 (1980).

[3] Y. Li and P. D. Sclavounos, "Three-dimensional nonlinear solitary waves in shallow water generated by an advancing disturbance", J. Fluid Mech. **470**, 383–410 (2002).

[4] J. Kevorkian and J. Yu, "Passage through the critical Froude number for shallow-water waves over a variable bottom", J. Fluid Mech. **204**, 31–56 (1989).

[5] L. G. Redekopp and Z. You, "Passage through resonance for the forced Korteweg-de Vries equation", Phys. Rev. Lett. **74**, 5158–5161 (1995).

[6] R. Grimshaw, E. Pelinovsky, and P. Sakov, "Interaction of a solitary wave with an external force moving with variable speed", Stud. Appl. Math. **97**, 235–276 (1996).

[7] T. Jiang, R. Henn, and S. D. Sharma, "Wash waves generated by ships moving on fairways of varying topography", in *Proceedings for the 24th Symposium on Naval Hydrodynamics* (Fukuoka, Japan) (2002).

[8] T. Y. Wu, "Long waves in ocean and coastal waters", J. Eng. Mech. Div. ASCE **107**, 501–522 (1981).

[9] G. Pedersen, "Three-dimensional wave patterns generated by moving disturbances at transcritical speeds", J. Fluid Mech. **196**, 39–63 (1988).

[10] S. Lee, G. Y. Yates, and T. Y. Wu, "Experiments and analysis of upstream-advancing solitary waves generated by moving disturbances", J. Fluid Mech. **199**, 569–593 (1989).

[11] D. D. Houghton and A. Kasahara, "Nonlinear shallow fluid flow over an isolated ridge", Commun. Pure Appl. Math. **XXI**, 1–23 (1968).

[12] B. T. Nadiga, L. G. Margolin, and P. K. Smolarkiewicz, "Different approximations of shallow water fluid flow over an obstacle", Phys. Fluids **8**, 2066–2077 (1996).

[13] M. Tanaka, "The stability of solitary waves", Phys. Fluids, **29**, 650–655, (1986).

[14] Y. Cao, R. F. Beck, and W. W. Schultz, "Numerical computations of two-dimensional solitary waves generated by moving disturbances", Int. J. Numer. Meth. Fluids **17**, 905–920 (1993).